LAWRENCE
LIVERMORE
NATIONAL
LABORATORY

UCRL-JRNL-236518

Robustness Studies of Ignition Targets for the National Ignition Facility in Two Dimensions

D. S. Clark, S. W. Haan, J. D. Salmonson

November 13, 2007

Physics of Plasmas

Disclaimer

Robustness studies of ignition targets for the National Ignition Facility in two dimensions

Daniel S. Clark,* Steven W. Haan, and Jay D. Salmonson
Lawrence Livermore National Laboratory, Livermore, California 94550
(Dated: November 1, 2007)

Inertial confinement fusion capsules are critically dependent on the integrity of their hot spots to ignite. At the time of ignition, only a certain fractional perturbation of the nominally spherical hot spot boundary can be tolerated and the capsule still achieve ignition. The degree to which the expected hot spot perturbation in any given capsule design is less than this maximum tolerable perturbation is a measure of the ignition margin or robustness of that design. Moreover, since there will inevitably be uncertainties in the initial character and implosion dynamics of any given capsule, all of which can contribute to the eventual hot spot perturbation, quantifying the robustness of that capsule against a range of parameter variations is an important consideration in the capsule design. Here, the robustness of the 300 eV indirect drive target design for the National Ignition Facility [J. D. Lindl, *et al.* , Phys. Plasmas **11**, 339 (2004)] is studied in the parameter space of inner ice roughness, implosion velocity, and capsule scale. A suite of two thousand two-dimensional simulations, run with the radiation hydrodynamics code Lasnex, is used as the data base for the study. For each scale, an ignition region in the two remaining variables is identified and the ignition cliff is mapped. In accordance with the theoretical arguments of Levedahl and Lindl [Nucl. Fusion **37**, 165 (1997)] and Kishony and Shvarts [Phys. Plasmas **8**, 4925 (2001)], the location of this cliff is fitted to a power law of the capsule implosion velocity and scale. It is found that the cliff can be quite well represented in this power law form, and, using this scaling law, an assessment of the overall (one- and two-dimensional) ignition margin of the design can be made. The effect on the ignition margin of an increase or decrease in the density of the target fill gas is also assessed.

PACS numbers:

I. INTRODUCTION

Targets designed for inertial confinement fusion (ICF) ignition experiments on the National Ignition Facility (NIF) [1] have undergone a steady evolution in recent years. One factor driving this design evolution has been an effort to improve the overall robustness of the target design. Given that certain physical processes in the implosion dynamics, as well as the characteristics of the individual targets, will remain fundamentally uncertain (or at least not perfectly reproducible from shot to shot), the robustness of a target is broadly defined as the certainty with which a particular yield will be exceeded in the face of inevitable variability. More robust targets are more likely to give the desired yield, while less robust targets are less so. Moreover, if the target robustness with respect to a particular variable can be quantified and the range of variability in that variable can be bracketed, then the target ignition margin can be defined as the distance in parameter space from the expected value of that variable to the value at which ignition fails. For the same expected range of variability, target designs with larger margins are more robust and can be expected to burn reliably with substantial yield. Targets with smaller margins are less robust and more likely to "fizzle." The challenge in the context of the ignition targets, however, is that this capsule robustness must be assessed in an extremely high dimensional parameter space whose variables include virtually every characteristic of the given target: the capsule dimensions and composition, laser and hohlraum performance, possible uncertainties in material equations of state and opacities, etc. The central concept in the ignition margin is to encapsulate all of these many potential contributors to capsule robustness into a single, and hopefully fairly simple, predictor of whether a particular capsule design will robustly ignite.

Of the very many factors which can contribute to variabilities in the target yield, two broad categories nevertheless do emerge: variabilities which are essentially one-dimensional (1-D) in character and variabilities which are fundamentally 2-D or 3-D effects. 1-D variabilities include, for example, the capsule implosion velocity, the peak drive pressure, and the fuel entropy. Previous authors have investigated the dependence of the ignition margin on these 1-D factors, and from this work a 1-D ignition margin can be defined. Principle among the 2-D and 3-D effects are the initial roughnesses of the many interfaces in the radial composition of the target. It is well known that even very small imperfections at these interfaces can be hugely amplified by Rayleigh-Taylor (RT) and Richtmyer-Meshkov instabilities over the course of the implosion and lead to unacceptable levels of mixing between layers or even complete breakup of the target. Of particular concern, is the roughness of the inner fuel (ice) layer since it is this interface which forms the ultimate boundary between the very high temperature hot spot, where fusion ignition should occur, and the much colder main fuel layer. Substantial perturbations of this

*Electronic address:clark90@llnl.gov

hot spot-fuel boundary, principally due to the growth of RT spikes during the stagnation phase of the implosion, can result in an unacceptable cooling of the hot spot and eventual quenching of ignition. Some work has been done to quantify the impact of these 2-D and 3-D effects on the ignition margin. As complete an understanding as for the 1-D parameters affecting ignition, however, has yet to be established.

The central result of this paper is to extend previous 1-D work on quantifying ignition margins to include crucial 2-D effects. Given the interaction of the many complex and nonlinear physics processes in determining target yield, including 2-D hydrodynamic instability growth, a simulation-based approach is required. Here, a data set of two thousand 2-D implosion simulations, run with the radiation hydrodynamics code Lasnex [2], is assembled. In an effort to assess the ignition margin of a current NIF target design, the 300 eV, graded-doped beryllium capsule design is chosen as the baseline for the study. This design was then systematically varied through the parameters of capsule scale, peak implosion velocity, and hot spot perturbation at ignition. The resulting data set of simulations was then analyzed to extract a power law approximation for the ignition margin in the three implosion variables of scale, velocity, and fractional perturbation of the igniting hot spot. When assessed against the entirety of the data set, the margin power law was found to be a remarkably effective predictor of capsule yield. Tangentially, the effect of varying the initial fill gas density on robustness was also investigated.

This paper is organized as follows. The following section reviews previous work on minimum capsule ignition energies and their motivation of a definition for capsule ignition margin. Section III then describes the 300 eV NIF ignition design chosen as the baseline for this study and the characteristics of the 2-D simulations making up the data set. Section IV explains the methodology for scanning the baseline design through the three variables which contribute to the margin, and Sec. V summarizes the results of these parameter scans principally in the form of capsule yield versus implosion velocity and hot spot perturbation fraction. The analysis of this data set leading to a power law for the capsule margin is presented. Section VI then briefly addresses another variable which can impact the ignition margin of a design, the central gas fill density in the capsule. Section VII concludes.

II. PREVIOUS WORK

Foremost in quantifying capsule ignition margin is a precise definition of what is meant by margin. This is essentially the question of defining an appropriate metric for measuring distances in the capsule parameter space being investigated, a parameter space whose various coordinate axes (*e.g.*, entropy and implosion velocity) are not compatible in the traditional sense of having similar units. A rational and often-used definition of the ignition margin is simply the ratio of the kinetic energy available in a particular capsule design to the minimum energy required for ignition. This definition is particularly facilitated by the work of previous authors in quantifying the minimum capsule energy needed for ignition.

Several authors [3–8] have published power laws for minimum energy for ignition of the form

$$E_{\rm ign} \propto \alpha^a \, v^{-b} \tag{1}$$

where $E_{\rm ign}$ is the minimum fuel kinetic energy necessary for ignition, α is the in-flight fuel adiabat (or equivalently entropy), and v the peak fuel implosion velocity. Values as low as $a = 1.7$ and $b = 5.5$ [6, 9] or as high as $a = 3$ and $b = 10$ [3] have been proposed for these exponents. The most recent values for these exponents (and arguably the most definitive since they include most of the relevant 1-D physical phenomena) are $a = 1.88 \pm 0.05$ and $b = 5.89 \pm 0.12$ as given by Herrmann *et al.* [7]. Taking these values as approximating this minimum ignition energy requirement, the kinetic energy ignition margin in 1-D should be

$$M \doteq \frac{E_{\rm kin}}{E_{\rm ign}} \propto \frac{\frac{1}{2} m \, v^2}{v^{-5.9}} \propto R^3 v^{7.9} \tag{2}$$

where the fuel mass m is taken to scale as the cube of the capsule radius or scale R.

Since it is based on only 1-D analytic and simulation work, this power law of course omits any degradation of the margin due to 2-D or 3-D effects. To extend this definition of the ignition margin to included the effect of 2-D perturbations, Levedahl and Lindl [9] proposed the following modification: since any perturbations to the boundary of an igniting hot spot can be expected to cool the neighboring plasma and so prevent it from participating in the ignition process, such perturbed hot spots should be treated as hot spots of effectively smaller scale. If the hot spot radius is perturbed to some fraction $\xi \doteq 1 - R_{\rm 2D}/R_{\rm 1D}$, where $R_{\rm 1D}$ is the radius the hot spot would have had in the absence of perturbations and $R_{\rm 2D}$ is the radius of the hot spot subtracting the region that is cooled due to the perturbations, *i.e.*, a fraction $\eta \doteq 1 - \xi$ is left "clean" and unperturbed, then the hot spot radius has been effectively rescaled according to $R \to \eta \times R$. Using the 1-D margin formula in Eq. (2), a 2-D version of the margin formula should then be

$$M \propto R^3 v^{7.9} \eta^3 \, . \tag{3}$$

This argument was further refined by Kishony and Shvarts [10], who noted that a mode number dependence should be expected in the exponent of the clean fraction η. For perturbations from sphericity corresponding to low order Legendre modes, the RT bubbles surrounding the hot spot will be broad with centers well separated from the cold, interleaved spikes. The plasma enveloped by broad, low-mode bubbles may then yet contribute to the ignition of the hot spot and should not then be wholly

discarded from the ignition margin, as implied by the scaling leading to Eq. (3). An exponent on η different than 3.0 should be expected in this case. On the other hand, for high-mode perturbations of the same amplitude, the narrow bubbles will be more strongly cooled by the intervening spikes and so nearly all of the enveloped plasma is prevented from contributing to the hot spot. An η exponent closer to 3.0 should be anticipated for this case. In practice, of course, the perturbations of any given hot spot will be neither purely low mode nor purely high mode but the product of the growth of a random spectrum of initial modes combining low and high modes. To account for these mode number effects, as well as to include realistic treatments of the heat conduction from the hot spot, thermonuclear burn product deposition in the hot spot, etc., requires realistic full capsule simulations. The inclusion of all of these effects, as well as the need to assess the robustness of an ignition relevant capsule design with initial perturbation spectra and instability growth rates typical of what is anticipated for the ignition campaign, motivated the present simulation-based study.

III. BASELINE AND SIMULATION TECHNIQUE

The basis for this parameter study was the 300 eV NIF Be-ablator capsule design [11]. The capsule design consists of a 75 μm layer of deuterium-tritium (DT) ice encased in a graded-doped beryllium-copper ablator of 160 μm thickness to a total outer radius of 1000 μm. The five separate layers of the ablator are doped to copper concentrations of 0.0%, 0.35%, 0.7%, 0.35%, and 0.0% atomic with thicknesses of 5.0, 5.0, 50.0, 15.0, and 85.0 μm, respectively. These dopant concentrations and layer thickness were carefully chosen to manage the hydrodynamic flow profiles of the capsule throughout its implosion, and so control the growth of deleterious RT instabilities. The nominal capsule is held at a temperature of 18.0 K resulting in an equilibrium central gas fill of 0.3 mg/cm^3. Finally, the capsule is driven by a carefully tuned radiation pulse consisting of a sequence of four shocks and reaching a peak drive temperature of 300 eV. An example of this drive pulse is shown below in Fig. 3.

Since this study was undertaken, the NIF beryllium point design has evolved to a lower drive temperature (285 eV) and a larger capsule scale (1200 μm). Alternate ablator materials (germanium-doped plastic and high density carbon) also continue to be considered. Nonetheless, since the capsule margin formula given below is couched in terms of intensive capsule variables (the overall scale, implosion velocity, and the hot spot perturbation fraction), the formula should remain broadly applicable to these different capsule scales, ablators, and drive temperatures. Indeed, an appreciation of the capsule margin available in the 300 eV design in part motivated the redesign of this capsule to a 285 eV design which traded capsule margin for improved *Hohlraum* plasma conditions.

Like the capsule designs themselves, the techniques for simulating capsule performance using radiation hydrodynamics codes, such as Lasnex, are highly evolved. 2-D capsule instability simulations begin first with highly resolved 1-D simulations using both full multi-group radiation transport and multi-group radiation diffusion. The results of these high resolution simulations are then used to tune a less highly resolved 1-D simulation using a few group weighted opacity scheme with a mean-free-path-to-boundary correction. These less resolved, and hence much faster, simulations typically match the highly resolved simulations to within a percent in ablation rate, implosion history, and flow profiles. Full 2-D instability simulations, which complete in a reasonable run time, can then be evolved from these optimized 1-D simulations. All simulations were run using tabular opacities and equations of state.

IV. METHODOLOGY

To construct a data base of marginal capsules, the baseline capsule was systematically scanned in the parameters of scale, implosion velocity, and hot spot perturbation fraction. Performing a parameter scan in the first of these variables, the capsule scale, is easily accomplished simply by multiplying up or down by an overall factor all of the capsule dimensions as well as the timing of the radiation drive pulse. Characteristic of what total laser energies are reasonably achievable on NIF, rescalings to 0.9, 1.1, and 1.2 of the nominal 1.0 scale were chosen. These scales correspond approximately to total laser energies of 750 kJ, 1.3 MJ, and 1.6 MJ, respectively. Note that, in the process of multiplying all of the capsule dimensions, the perturbations on all of the capsule interfaces were keep to a constant physical amplitude.

There is, however, one subtlety in this rescaling procedure, namely that similar 1-D hydrodynamic flow profiles must be preserved in going from scale to scale. Since another quantity of interest in the scaling law is the degree of hot spot perturbation at ignition, which is in turn dependent on the degree of hydrodynamic instability growth during the course of the implosion, the capsules must have similar 1-D flow profiles (particularly ablation front gradients and Atwood numbers) from scale to scale so as to have comparable degrees of hydrodynamic instability. On the other hand, the 1-D flow profiles of the capsule are intimately dependent on the radiation transport through the capsule, a process which does not scale isomorphically with the capsules size. Hence, in order to preserve comparable degrees of hydrodynamic instability between capsule scales some compensation must be made in the radiation transport properties of the capsules. A simple means of compensating the radiation transport is to apply a multiplier to the copper concen-

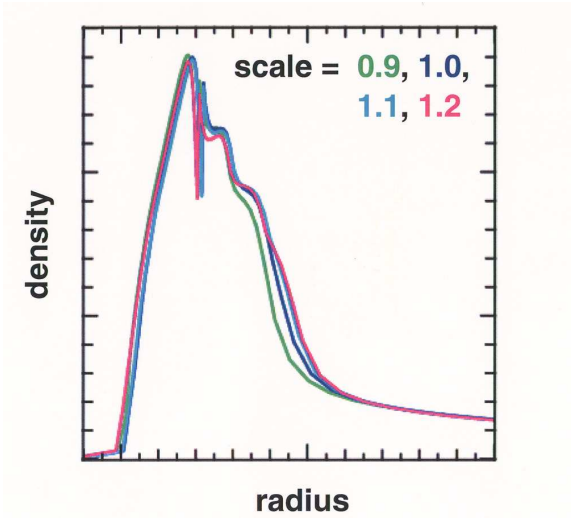

FIG. 1: (Color online) Shell density profiles for the four different scales after multiplying the copper concentration in the ablator at each scale according to Fig. 2. Each profile is plotted as a function of the rescaled radius at the time of peak implosion velocity. Similar Atwood numbers and ablation front density gradients indicate comparable degrees of hydrodynamic instability at each scale.

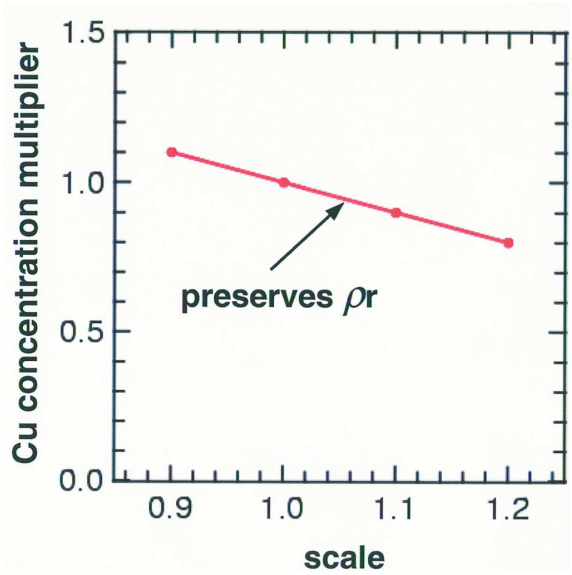

FIG. 2: (Color online) Multiplier on the ablator copper concentration to compensate for differing radiation transport with scale.

tration in the ablator as a function of scale. As illustrated in Figs. 1 and 2, by decrementing the copper concentration linearly with the capsule scale, the capsule density profiles (after rescaling the radii) can be made to match quite closely at the time of peak velocity. Physically, this linear decrement of the copper concentration as a function of scale simply reflects preserving the total capsule optical depth (integrated ρr). Of course, altering the

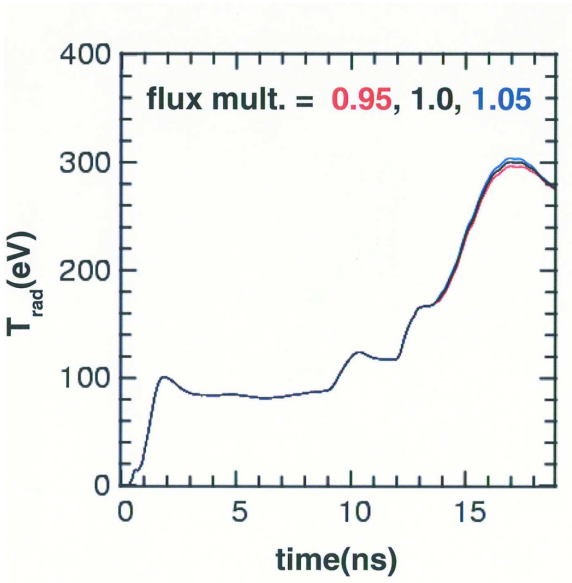

FIG. 3: (Color online) Radiation temperature versus time for driving the 300 eV design. Examples of a 5% increase and decrease in the peak radiation flux are also shown.

capsule composition in this way, as well as rescaling the capsule dimensions, sufficiently modifies the capsule radiation transport that the radiation drive must be retuned for each scale. This process entails repeating the procedure for generating an optimized 1-D implosion from a highly resolved transport simulation described above. As discussed further below, it is also impossible in this procedure to preserve exactly the fuel entropy from scale to scale since it is very sensitively dependent on the timing of the radiation drive. Some variation of the fuel entropy was inevitably introduced into the data set in this way.

To accomplish the scan in the second variable entering the margin scaling law, the peak implosion velocity, a multiplier was again applied to the nominal capsule, in this case to the peak radiation flux. This variation of the capsule implosion velocity with peak flux is illustrated in Figs. 3 and 4. For each scale, by multiplying the peak flux down in 5% increments, the implosion velocity was reduced until the capsule failed. As illustrated in Fig. 4, the location of this velocity cliff moves to lower velocities with increasing scale. A flux decrement of only approximately 15% is sufficient to quench the ignition of nominal capsule. For completeness, increasing the peak flux by 5% was also included in the parameter scan. Like the scan of the capsule scale, varying the capsule drive impacts the capsule radiation transport properties and with it the fuel entropy. This secondary entropy variation will again be taken into account below in the analysis leading to the margin power law.

Note that some variation in the peak drive pressure, another variable found to contribute to the minimum ignition energy in 1-D [7], might also be expected from varying the peak flux. It was found, however, that such

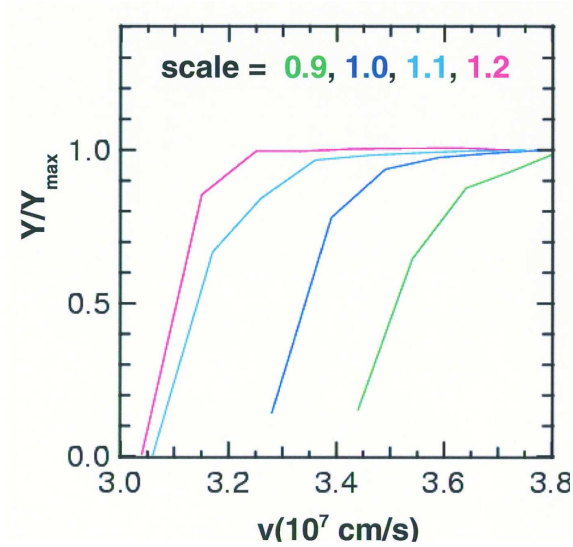

FIG. 4: (Color online) Yield curves in 1-D as a function of scale and implosion velocity obtained by multiplying the peak radiation flux. The nominal implosion velocity is 3.7×10^7 cm/s.

pressure variations were only very weak and negligible by comparison with the fluctuations between each realization of a given run. Given, additionally, that the 1-D margin depends only weakly on this peak pressure, this effect on the margin was deemed negligible.

Finally, the third parameter entering the margin power law, the hot spot perturbation fraction, was scanned by applying a multiplier to the roughness of the inner surface of the DT ice. In the 2-D instability simulations which make up the data set, roughnesses according to the NIF specification were included on all of the capsule interfaces (including the dopant layers in the ablator). Since it has the most direct impact on the ultimate hot spot perturbation, however, only the roughness of the ice was varied. The nominal roughnesses of the inner ice surface and the other capsule interfaces (fuel-ablator, the four internal layers of the ablator, and the outer surface of the ablator) were 1.0 μm, and 200 nm, respectively. In order to capture some of the statistical variability of the surface roughness, simulations with equal ice roughnesses were repeated six times with different randomly phased perturbation spectra for each interface. The averages and error bars which appear below are computed form these six equivalent realizations of the same surface roughness. As can be anticipated, the error bars are generally small for robustly burning capsules and large on the ignition cliff where the greatest sensitivity and variability are expected. Finally, the 2-D simulations included sufficient resolution only to capture surface perturbations corresponding to Legendre modes $1-30$. Given that, *a posteriori*, the dominant hot spot perturbations were observed to occur at modes $8-12$, this limited resolution in mode number should not compromise the fidelity of the data base.

While it is the initial ice roughness which is varied from run to run, it is the perturbation fraction of the hot spot at stagnation that is relevant to the margin power law. A prerequisite, then, to analyzing the simulation data base is a robust definition of the hot spot shape or boundary. Robustly defining the boundary of the igniting hot spot is not as straightforward as it may seems, however, precisely because a definition must be found which works reliably for capsules which are failing. Such capsules necessarily have highly distorted hot spots with boundaries that are not easily defined. From examining a subset of the implosions constituting the data base, it was apparent that the contour of no single hydrodynamic variable (*e.g.*, the shell density, the ion temperature, or the thermonuclear burn rate) captures the intuitive sense of the hot spot in these highly distorted cases. Fig. 5 illustrates this: To the eye, a reasonable hot spot boundary is apparent. For this marginal hot spot, however, (with six times the nominal ice roughness) the half-maximum density contours (shown in magenta) do not form a closed contour. This is due to the nonlinear development of the RT instability poking holes through the stagnating shell. Likewise, the ion temperature contours (shown in cyan) can be not simply connected and include islands of high temperature isolated from the main hot spot. Finally, the contour of the thermonuclear energy production rate (shown in black), while forming a simply closed contour, appears to over-smooth the hot spot shape and underrepresent the distortion of the core. Indeed, from the perspective of assessing the effect of hot spot perturbations on ignition, the energy production rate deserves best to be classified as characterizing an effect of the hot spot perturbations rather than as a metric for the degree of perturbation.

To quantify the perturbation fraction in these highly distorted hot spots, then, the following hybrid definition was developed: the hot spot boundary was defined as the contour which encloses the half-maximum density contour truncated by the contours where the ion temperature equaled 1.0 keV and the thermonuclear energy production rate became positive. Fig. 6 illustrates that, for the highly distorted hot spot from Fig. 5, where no single contour reasonably tracked the intuitive sense of the hot spot boundary, this hybrid definition readily follows that boundary. For comparison, Fig. 6 also illustrates the far less distorted hot spot corresponding to the nominal capsule. In this less extreme case, the hot spot boundary defaults essentially to the half-maximum density contour. Finally, it should be emphasized that no special physical significance is meant to be attached to this hot spot definition. It was merely observed as a matter of trial and error that this definition worked for very nearly every member of the subset of hot spots examined.

Once a robust definition of the hot spot boundary was found, the hot spot perturbation fraction could then be measured for each realization of the implosion at each scale, velocity, and roughness. Here, the hot spot pertur-

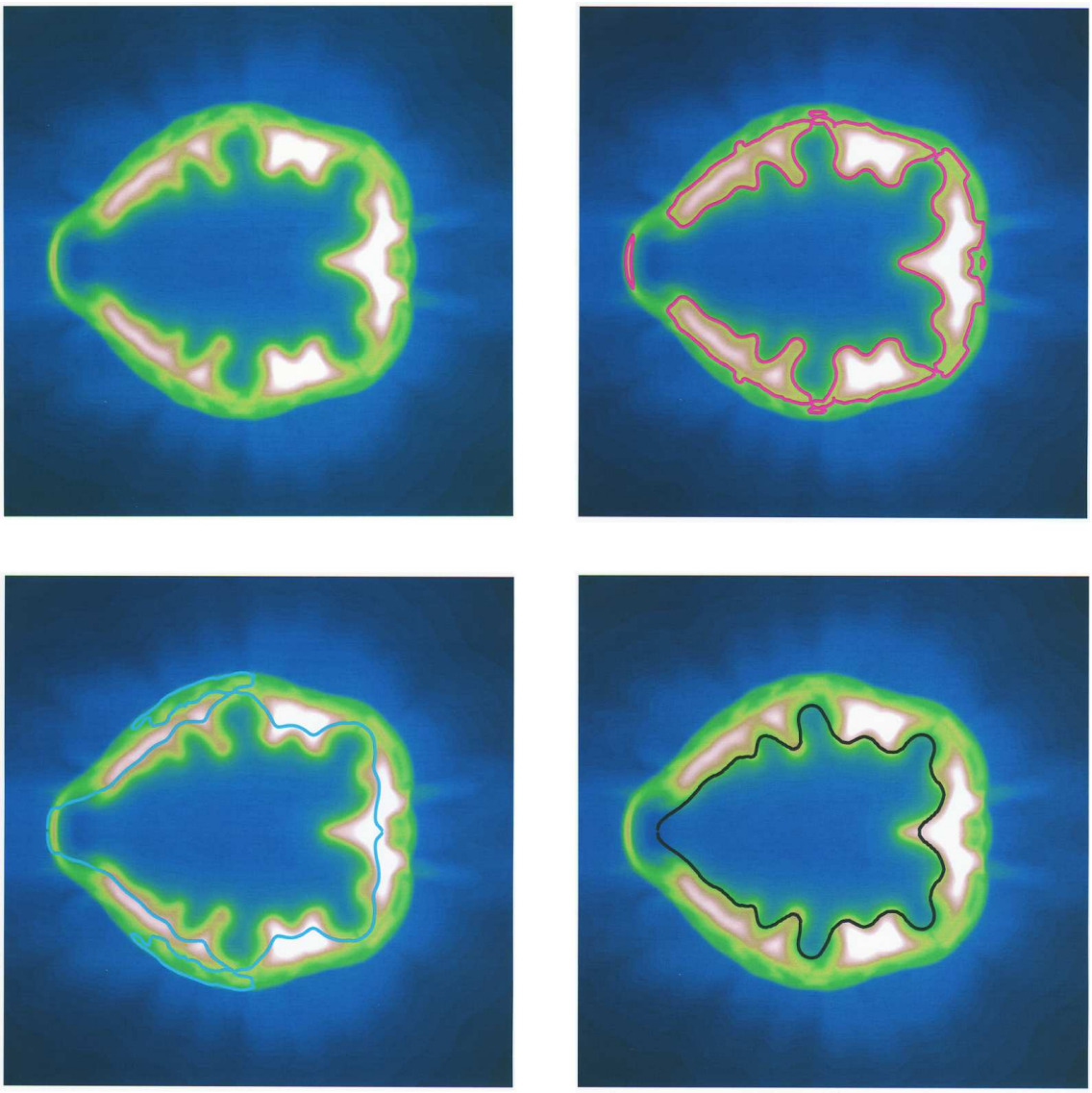

FIG. 5: (Color online) Example of a highly distorted hot spot at ignition time. The color scale gives the relative density. The magenta curve is the half-maximum density contour, the cyan curve is the 1.0 keV ion temperature contour, and the black curve is the contour of 1%-maximum thermonuclear energy production rate. Only the last forms an acceptably closed contour but still fails to capture the true hot spot shape.

bation fraction was computed as the root mean square (RMS) deviation of the hot spot radius at each point on the boundary from the average over all of the boundary points. A weight was included by the cosine of the polar angle to account for the larger solid angle (in 3-D) subtended by the perturbations near the capsule waist than at the poles. As Fig. 7 illustrates, the hot spot perturbation fraction increases approximately linearly with the initial roughness of the ice surface for each of the four scales examined. The error bars again represent averages of the six realizations of each roughness. As anticipated, the error bars are small for the weakly perturbed capsules, which burn robustly, but large for the strongly perturbed capsules located on the ignition cliff. In an effort to minimize such fluctuations in the data, the hot spot perturbations shown in Fig. 7 were measured at the ignition time of the corresponding 1-D simulation, not at the ignition time from the 2-D perturbed simulation. Here, the ignition time was defined as the time at which the central ion temperature first exceeded 12.0 keV. Similarly, the hot spot perturbation fraction was computed by normalizing the hot spot RMS to the radius of the hot spot from the equivalent 1-D simulation. In this sense, the measured hot spot perturbation fraction indeed represents the intended deviation of the 2-D capsule from its corresponding 1-D ideal.

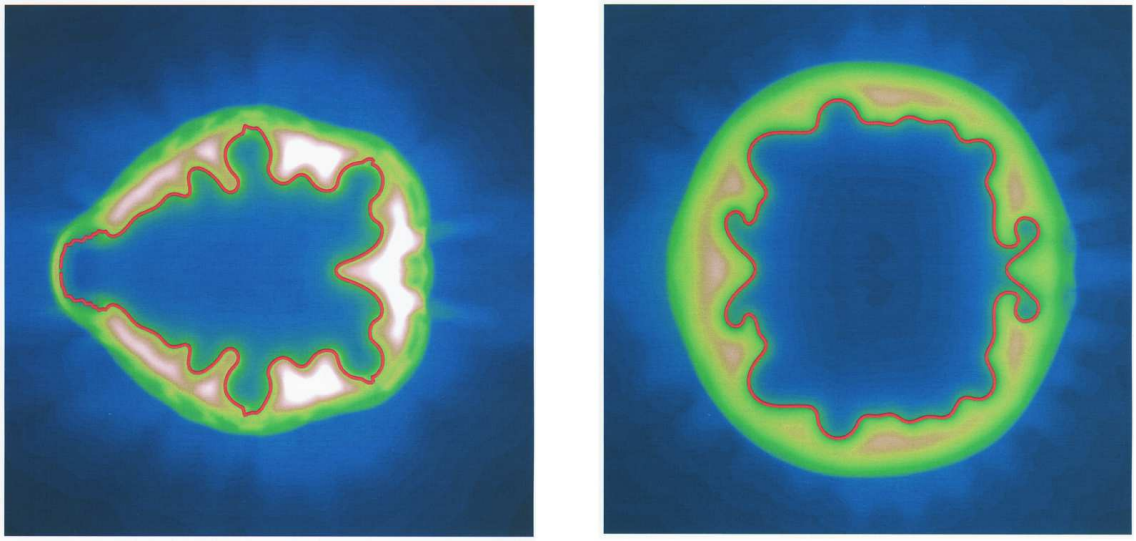

FIG. 6: (Color online) The same hot spot as in Fig 5 but with the hot spot demarcated using the hybrid hot spot definition. This definition closely tracks the details of the true hot spot shape. For comparison, the much less distorted hot spot of the nominal capsule design is shown on the right.

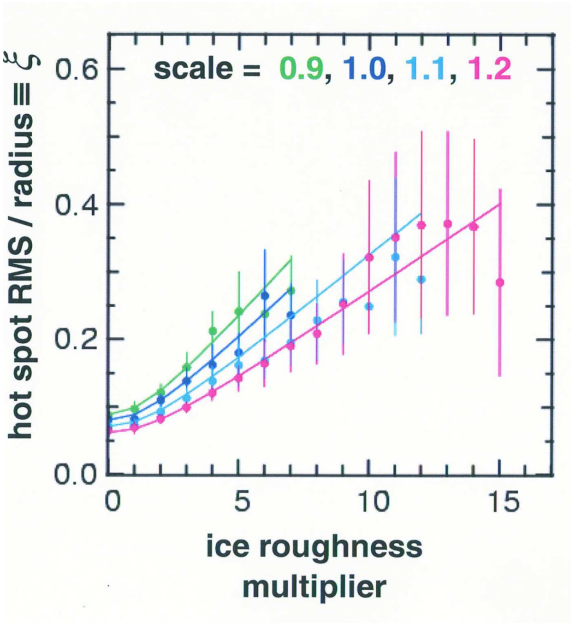

FIG. 7: (Color online) Hot spot perturbation fraction as a function of multiplier on the initial roughness of the DT ice. The implosion velocity is the nominal 3.7×10^7 cm/s.

V. DATA BASE RESULTS AND SCALING LAWS

The complete data set consists of velocity and hot spot perturbation scans for each of the four different scales. Fig. 8 plots the capsule yields from the data base in the velocity-perturbation fraction plane at each scale. The yield is predictably close to the 1-D value when the velocity is high and the perturbation fraction small and is low where the perturbation fraction is high and the velocity low. It is also immediately evident from the figure that the scale 0.9 capsule is relatively very marginal, with only a small region in parameter space where the yield is significant. Conversely, the scale 1.2 capsule is relatively very robust with a large region of substantial yield. Between the extremes of near 1-D and essentially negligible yield, each frame in Fig. 8 also shows a region of rapid yield variation corresponding to the ignition cliff. As the implosions on this ignition cliff are, by definition, marginal, it is the location of this cliff that is the crucial ingredient to the margin power law.

To quantify the location of the ignition cliff, marginal capsules were defined as those giving a yield of 1 MJ. Note that this definition is distinct from the definition used by Herrmann *et al.* [7] in their work on minimum ignition energy scaling laws. They chose to define marginal capsules as those with yield equal to the capsule absorbed energy which, in practice, amounts to $Y \simeq 160$ kJ. The different definition used here was motivated by the reality, in 2-D, that the data set showed unacceptably large fluctuations when the implosions were so strongly perturbed as to yield ~ 100 kJ.

Having defined marginal capsules as those with $Y = 1$ MJ, the location of the ignition cliff was mapped as the critical perturbation fraction which duded the capsule to this yield at each scale and velocity. As illustrated in Fig. 9, this critical perturbation fraction was computed from averaging the result from the yield curves for each of the six realizations of a run as the initial ice roughness was increased. Note that reducing the definition of a marginal capsule from 1 MJ to the ~ 100 kJ definition would substantially increase the uncertainty in the value of the critical perturbation fraction.

Once the critical perturbation fractions have been tab-

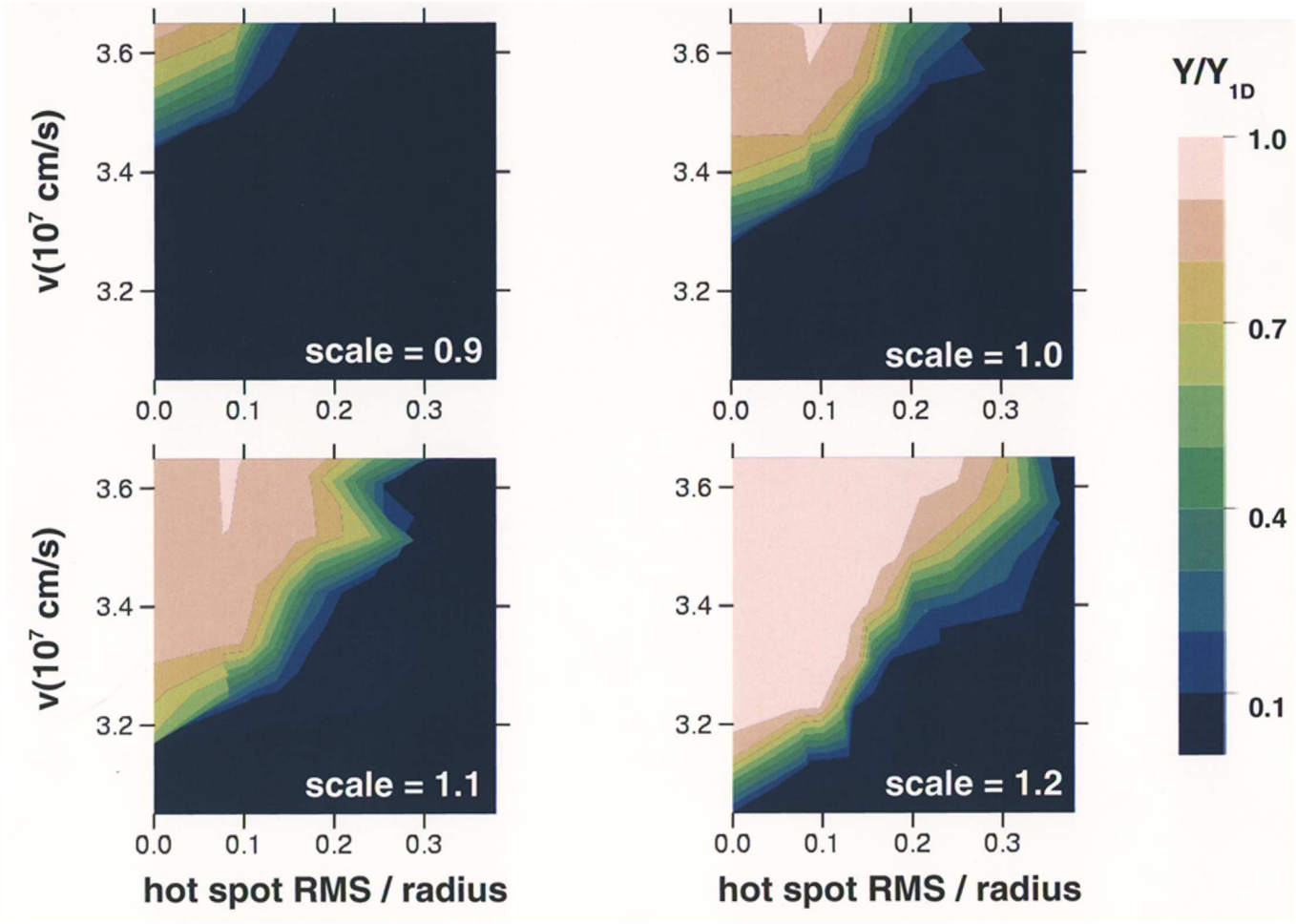

FIG. 8: (Color online) The complete 2-D data set plot as capsule yield versus implosion velocity and hot spot perturbation fraction. Capsule yields are close to the 1-D values for high velocities and low perturbation fractions and fall precipitously for low velocities or large perturbations. The scale 0.9 capsule is clearly very marginal and the scale 1.2, comparatively, quite robust.

ulated for each scale and velocity, the data may be fit to give a power law for the margin. However, the variability of the fuel entropy, noted in Sec. IV, must first be accounted for. From the previous work on capsule ignition energy [3–7], it is known that the minimum ignition energy (and hence also the ignition margin) is a very strong function of the fuel entropy or adiabat. Ideally, then, if a power law fit is to be found for the margin as a function of the scale, velocity, and perturbation fraction, the entropy should be held constant across the various scales, velocities, and perturbation fractions. Unfortunately, for the reasons given above in Sec. IV and illustrated in Fig. 10, this is not the case in the 2-D data set. As the capsule scale was varied the average fuel entropy systematically fell. This, again, is an illustration of the scale dependence of the radiation transport. Alternately, as the peak flux multiplier was reduced, the average entropy systematically increased due to the altered timing of the radiation drive. The variations in the entropy are evidently only at the level of percent; however, given the extreme sensitivity of the margin to the entropy, such variations cannot be neglected.

In principle, these 1-D variations in the entropy may be compensated for in the 2-D data set using the scalings of the minimum ignition energy found in 1-D [3–7]. That is, since Eq. (1) effectively relates the adiabat (or entropy) to velocity at constant ignition energy (or margin), increases in the entropy may be accounted for as a proportionate reduction in velocity. Since it is more closely connected to the work at hand, however, a power law fit from the work of Salmonson *et al.* [12] was chosen to compute this correction. Salmonson *et al.* assembled a data set of 10,000 1-D simulations obtained by randomly varying thirty-four 1-D capsule parameters. A central result of this study was that, from the thirty-four 1-D sources of yield degradation allowed, the yield was found dominantly to be determined by the two variables of the fuel-averaged entropy S and implosion velocity v. Germain to the data set of 2-D marginal capsules, the 1 MJ contour representing these marginal capsules was found

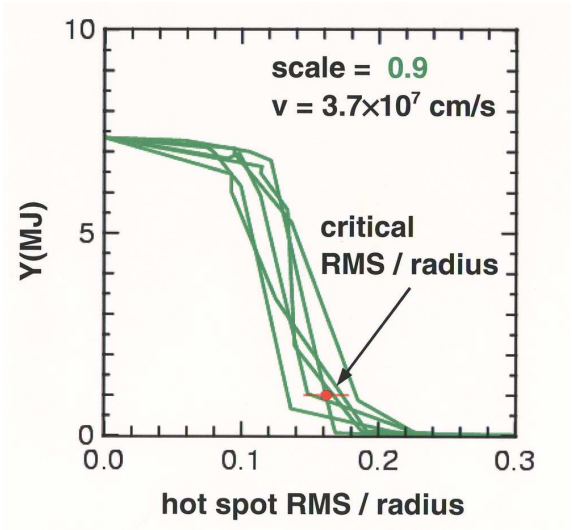

FIG. 9: (Color online) An example set of yield curves from six realizations of the scale 0.9 capsule with the nominal implosion velocity. The critical hot spot perturbation fraction giving $Y = 1\,\mathrm{MJ}$, and its associated error bar, is shown by the red dot.

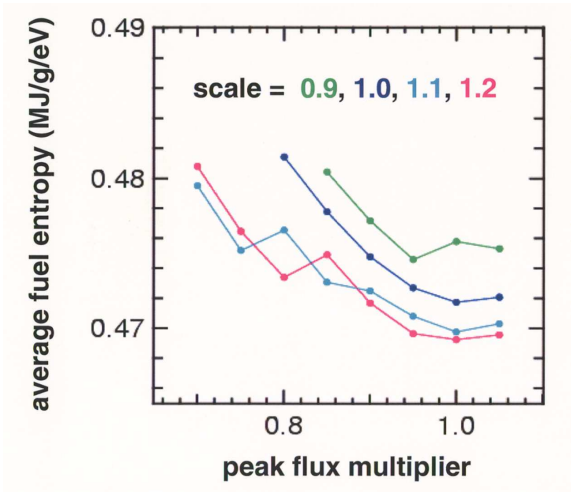

FIG. 10: (Color online) 1-D entropy variations in the data set plotted as a function of peak flux multiplier and scale. The entropy is a decreases with scale due to the reduced fuel preheat and increases with decreasing flux multiplier due to the modified drive timing.

to be fit quite well by the power law $v \propto S^{1.2}$. To compensate the observed entropy variations in the 2-D data set, then, the 2-D implosion velocities should be decremented according to $v \to v \times S^{-1.2}$, with S the measured 2-D fuel entropies from Fig. 10.

Accounting for this effect of the entropy, the 2-D critical perturbation fraction may now be fit as a power law in the reduced velocity and scale

$$1 - \frac{\text{critical RMS}}{\text{radius}} \equiv \eta \propto R^a \left(v\, S^{-1.2}\right)^b$$

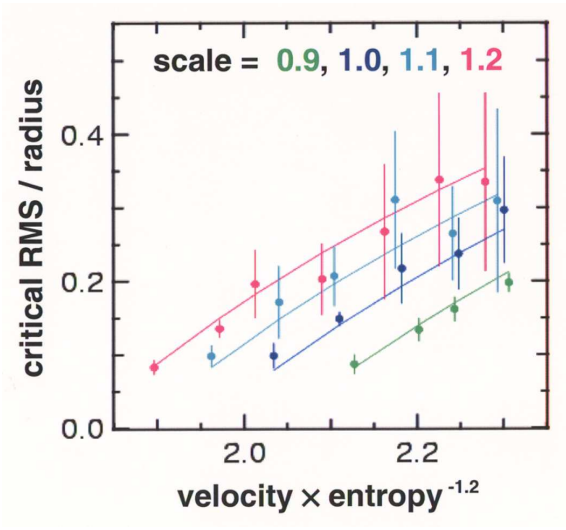

FIG. 11: (Color online) Data base results of critical perturbation fraction versus reduced velocity and scale. The power law fit from Eq. (4) represents the data well.

where, again, $\eta \equiv 1 - \xi$ denotes the fraction of the hot spot which is "clean." By taking the logarithm of this equation, the exponents may be determined by a simple least squares linear fit to the data [13]

$$\ln \eta = a \ln R + b \ln\left(v\, S^{-1.2}\right) + \text{const.}$$

After weighting the data points inversely with the error bars, the resulting exponents are

$$\begin{aligned} a &= -0.75 \pm 0.04 \\ b &= -1.87 \pm 0.07 \\ \text{const.} &= -11.68 \pm 0.45\,. \end{aligned} \tag{4}$$

The reduced χ^2 for the fit was 0.62 indicating that a power law is in fact a reasonable representation of the data. As can be verified from Fig. 11, this fit does indeed pass through the error bars of the data for all but one point.

The power law fit for the $Y = 1\,\mathrm{MJ}$ surface from the data set is then

$$\eta \propto R^{-0.75\pm0.04}\, v^{-1.87\pm0.07}\, S^{2.25\pm0.09}$$

which may, of course, be rewritten as

$$\text{const.} = R^{-0.75\pm0.04}\, v^{-1.87\pm0.07}\, S^{2.25\pm0.09}\, \eta^{-1}\,. \tag{5}$$

By definition, however, the $Y = 1\,\mathrm{MJ}$ surface fit by Eq. (5) corresponds to the surface where $M = 1$. It is an immediate consequence, then, that the constant on the left side of Eq. (5) must be proportional to a power of the margin. That is, the sought-for margin power law must be some power of Eq. (5), *i.e.*,

$$M \propto \left[R^{-0.75\pm0.04}\, v^{-1.87\pm0.07}\, S^{2.25\pm0.09}\, \eta^{-1}\right]^p$$

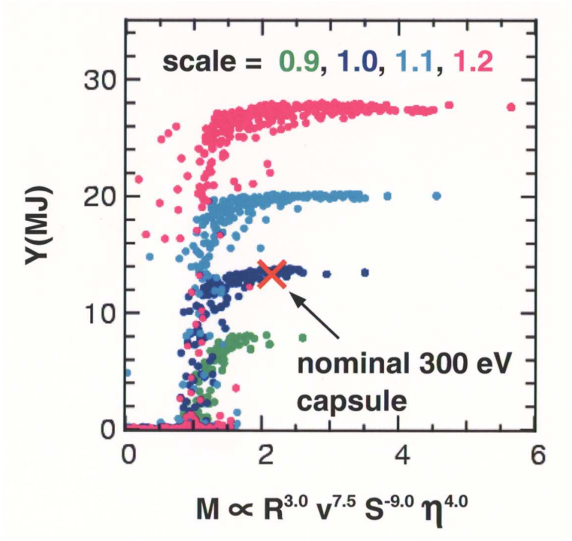

FIG. 12: (Color online) The entire data set of 2-D simulations plotted as Yield versus the margin power law in Eq. (6). Aside from a minority of outliers, the simulations are aligned predominately onto a single ignition cliff.

with p an arbitrary power. Finally, this overall power may be determined by appealing to the original definition of the capsule margin from Sec. II. There the margin was defined as the ratio of the available kinetic energy to the minimum energy needed for ignition. Since the capsule kinetic energy must be proportional to the capsule mass, which in turn must be proportional to the cube of the capsule radius, it is then required that

$$M \doteq \frac{E_{\rm kin}}{E_{\rm ign}} \propto m \propto R^{3.0}\,.$$

Reconciling these two expressions for M determines the value of p, so that

$$M \propto R^{3.0}\, v^{7.51\pm0.38}\, S^{-9.01\pm0.45}\, \eta^{4.01\pm0.24}\,. \qquad (6)$$

Eq. (6) is the central result of this paper.

Fig. 12 plots the entire data set of 2-D simulations in the plane of capsule yield versus the margin parameter from Eq. (6). That this form for the margin neatly aligns the entire data set (spanning different capsule scales, velocities, and perturbation fractions) onto a single ignition cliff is clearly evident. For orientation, the location of the nominal 300 eV capsule design from which the data set was generated is shown as the red "X" at a margin of 2.1. Some outliers with $M < 1$ and $Y > 1\,$MJ or $M > 1$ and $Y < 1\,$MJ, of course, remain but constitute less than 2% of the entire data set. On individual inspection, all of these outliers are found to be located on an ignition cliff, either in perturbation fraction or velocity, where greater sensitivity, and hence variability, can be expected.

In the figure, the overall multiplicative constant in the margin has been chosen to align the ignition cliff with the location of $M = 1$. When normalized to their nominal values, the margin power law then takes the form

$$M = 2.1 \left(\frac{R}{1\text{mm}}\right)^{3.0} \left(\frac{v}{3.7\times10^7\,\text{cm/s}}\right)^{7.5} \times \left(\frac{S}{0.47\,\text{MJ/g/eV}}\right)^{-9.0} \left(\frac{\eta}{0.92}\right)^{4.0}. \qquad (7)$$

Salient in this equation are two features: First, the scaling of the margin with velocity in 2-D, $v^{7.5}$, is encouragingly close to (and within the error bars of) the value found by Herrmann *et al.* in 1-D, namely, $v^{7.9}$. Secondly, the scaling of the margin with the hot spot clean fraction, $\eta^{4.0}$, is significantly greater than the value suggested by the scaling arguments of Levedahl and Lindl of $\eta^{3.0}$. This difference doubtless indicates the substantial role played by non-ideal processes in marginal ignition. Of course, error bars remain on the exponents in Eq. (7) and these values will likely continue to be refined as the data sets of 1-D and 2-D simulations expand and capsule designs continue to evolve.

VI. EFFECT OF FILL GAS DENSITY ON ROBUSTNESS

Another factor influencing the ignition margin of ICF capsules is the initial gas fill density in the capsule center. Increasing the central fill density reduces the ultimate convergence ratio of the capsule at stagnation, *i.e.*, increases the hot spot radius. Since the convergence ratio is reduced, less hydrodynamic instability growth can be expected with increased fill density, and hence capsule margin might be expected to increase with the gas fill. Counter acting this effect, however, is that the hot spot mass also increases with fill density. For a fixed hydrodynamic energy investment, eventually, with increasing gas fill, the hot spot will be too massive to reach ignition temperatures and the capsule will fizzle. If this effect proves strong enough, the margin will actually decrease with fill density. A further complication to this picture is that the innate roughness of the inner ice layer is expected to decrease with increasing capsule temperature resulting in a potential increase in the margin. Concomitant with the increased fielding temperature, though, is an increased fill density, which could have a detrimental effect on the margin. Again, the precise trade off between these effects can only be resolved in realistic 2-D simulations.

Using the methodology laid out in the previous sections, the effect of increasing and decreasing the fill gas density of the nominal capsule design was then assessed. For the four scales considered above (0.9, 1.0, 1.1, and 1.2), the critical hot spot perturbation fraction was determined at gas fill densities of $0.15\,\text{mg/cm}^3$ and $0.5\,\text{mg/cm}^3$ in addition to the nominal density of $0.3\,\text{mg/cm}^3$. The implosion velocity was held fixed for these simulations at the nominal value of $3.7\times10^7\,$cm/s. Fig. 13 summarizes these results for the three different fill densities.

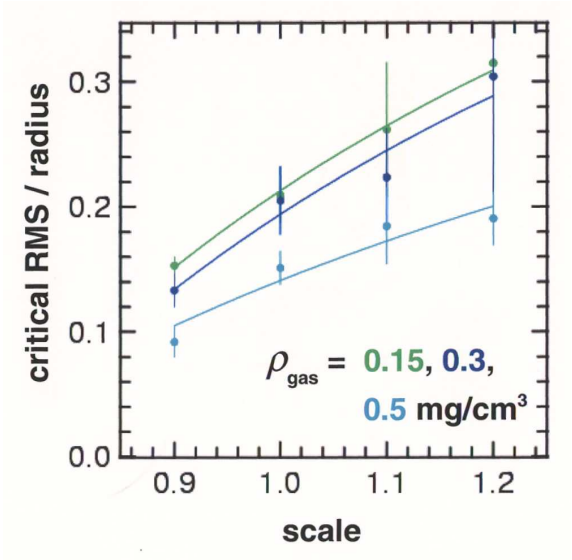

FIG. 13: (Color online) Critical hot spot perturbation fraction for $Y = 1\,\mathrm{MJ}$ plotted as a function of scale for the three gas fill densities $0.15\,\mathrm{mg/cm^3}$, $0.3\,\mathrm{mg/cm^3}$ (nominal), and $0.5\,\mathrm{mg/cm^3}$. At each scale, the critical perturbation fraction decreases approximately inversely with the fill density.

At each scale, the critical hot spot perturbation fraction which reduces the yield to 1 MJ is seen to increase approximately inversely with the central gas density. From the figure, increasing the temperature to the point that the gas fill reaches $0.5\,\mathrm{mg/cm^3}$ sufficiently degrades the allowable perturbation fraction to make this route to higher capsule margin uninteresting. Comparable tolerance to perturbations at the higher density (but with the same nominal perturbation fraction) would require an increase in scale from 1.0 to 1.2, effectively an increase in laser energy from 1.0 MJ to 1.6 MJ.

VII. CONCLUSIONS

In summary, a data set of two thousand 2-D Lasnex simulations has been assembled based on the 300 eV NIF point design. The data set systematically scanned this design in the parameters of capsule scale, peak implosion velocity, and hot spot perturbation fraction. From this data set, a power law for the critical hot spot perturbation fraction (the perturbation which reduced the yield to 1 MJ) was extracted in the implosion velocity and capsule scale. This power law was then converted into a power law for the ignition margin, defined as the ratio of the available capsule kinetic energy to the minimum energy required for ignition. This power law took the form

$$M \propto R^{3.0}\, v^{7.51\pm0.38}\, S^{-9.01\pm0.45}\, \eta^{4.01\pm0.24}\,.$$

When assessed against the entirety of the data set of 2-D simulations, this margin parameter proved to be an effective predictor of robust capsule burn. The power law additionally compares favorably in its velocity scaling with the 1-D work of Herrmann *et al.* [7] but shows stronger dependence on the hot spot perturbation fraction than anticipated by the rescaling arguments of Levedahl and Lindl [9] and Kishony and Shvarts [10]. In addition, increasing and decreasing the central fill gas density was also investigated.

While the results presented in this paper should extend previous understanding of the ignition margin by the inclusion of essential 2-D effects, further possible improvements yet remain. Foremost, the development of RT instabilities in ICF capsules, of course, occurs in three dimensions not in the 2-D idealization used in this study. That the very marginal hot spots, such as that shown in Fig. 5, show evidence of the nonlinear phase of RT growth, where the 2-D and 3-D developments differ, particularly motivates investigating capsule margins in 3-D. This modification of the margin due to 3-D effects is particularly acute in that weakly nonlinear RT growth is well-known to develop faster in 3-D than in 2-D [14]. However, assessing the capsule margin using suites of fully 3-D simulations, analogous to the data set of 2-D simulations used here, remains computationally very intensive and is likely only at the edge of the current state of the art.

Assessing the ignition margin of alternate capsule designs, using the same methodology as this study, as well as investigating the particular modal content of the hot spots in this study and its correlation with capsule robustness are other possibly fruitful avenues of research.

Acknowledgments

This work was performed under the auspices of the U. S. Department of Energy by Lawrence Livermore National Laboratory under Contract DE-AC52-07NA27344.

[1] J. D. Lindl, P. Amendt, R. L. Berger, et al., Phys. Plasmas **11**, 339 (2004).
[2] G. B. Zimmerman and W. L. Kruer, Comments Plasma Phys. and Controlled Fusion **2**, 51 (1975).
[3] J. Meyer-ter-Vehn, Nucl. Fusion **22**, 561 (1982).
[4] M. D. Rosen, J. D. Lindl, and A. R. Thiessen, in *Laser Programs Annual Report — 1983* (Lawrence Livermore National Laboratory, Livermore, CA, 1984), p. 5.
[5] M. M. Basko, Nucl. Fusion **35**, 87 (1995).
[6] M. M. Basko and J. Johner, Nucl. Fusion **38**, 1779 (1998).
[7] M. C. Herrmann, M. Tabak, and J. D. Lindl, Nucl. Fusion **41**, 99 (2001).
[8] A. Kemp and J. Meyer-ter-Vehn, Phys. Rev. Lett. **86**,

3336 (2001).
[9] W. K. Levedahl and J. D. Lindl, Nucl. Fusion **37**, 165 (1997).
[10] R. Kishony and D. Shvarts, Phys. Plasmas **8**, 4925 (2001).
[11] S. W. Haan, M. C. Herrmann, T. R. Dittrich, A. J. Fetterman, M. M. Marinak, D. H. Munro, S. M. Pollaine, J. D. Salmonson, G. L. Strobel, and L. J. Suter, Phys. Plasmas **12**, 056316 (2005).
[12] J. D. Salmonson (2008).
[13] P. R. Bevington, *Data Reduction and Error Analysis for the Physical Sciences* (McGraw-Hill, New York, 1969).
[14] D. Layzer, Astrophysical. J. **122**, 1 (1955).